EFFECT OF A DISTRIBUTED HEAT SOURCE ON MELT POOL GEOMETRY AND MICROSTRUCTURE IN BEAM-BASED SOLID FREEFORM FABRICATION

Srikanth Bontha and Nathan W. Klingbeil
Department of Mechanical and Materials Engineering
Wright State University
Dayton, OH 45435

Abstract

The ability to control geometric and mechanical properties of parts fabricated using laser-based manufacturing processes requires an understanding and control of melt pool geometry and microstructure. With the development of electron beam manufacturing or future beam-based deposition processes, the user may have more control over the distribution of incident energy, so that beam width becomes a potential process variable. As such, the focus of this work is the effect of a distributed heat source on melt pool geometry (length and depth) and the thermal conditions controlling microstructure (cooling rates and thermal gradients) in beam-based solid freeform fabrication. Previous work by the authors has employed the Rosenthal solution for a moving point heat source to determine the effects of process variables (laser power and velocity) on solidification cooling rates and thermal gradients controlling microstructure (grain size and morphology) in laser-deposited materials. Through numerical superposition of the Rosenthal solution, the current work extends the approach to include the effects of a distributed heat source for both 2-D thin-wall and bulky 3-D geometries. Results suggest that intentional variations in beam width could potentially enable significant changes in melt pool geometry without affecting microstructure.

Introduction

Over roughly the past decade, a number of laser-based material deposition processes have been developed for automatic fabrication of complex parts, adding features to existing parts, or repair of worn components. However, the widespread commercialization of these processes will ultimately require the ability to predict and control melt pool size, residual stress and microstructure through changes in process variables (e.g., laser power and velocity) [1]. With the advent of electron beam manufacturing or other next-generation processes, designers may have increased control over the distribution of incident energy compared to laser-based manufacturing. As a result, the ability to change the distribution of power (e.g., through changes in beam width) represents an additional process variable.

Among the key deposit characteristics, the control of melt pool size assumes the highest priority within the manufacturing community. This is because a consistent melt pool size is needed before specific features can even be built. At the same time, the control of microstructure is also critical, particularly in aerospace and other structural applications that have strict guidelines on resulting mechanical properties. While the control of melt pool size and solidification microstructure have been addressed in the literature [2], their interconnection has yet to be fully investigated. In particular, it has not been shown how changing process variables to control melt pool size might simultaneously affect cooling rates and thermal gradients which ultimately control microstructure.

To this end, the current study investigates how changes in laser or electron beam width simultaneously affect melt pool geometry and microstructure in beam-based solid freeform fabrication.

The approach is based on superposition of the well known Rosenthal solution for a moving point heat source traversing an infinite substrate [3], which has found extensive application in the literature. While the Rosenthal solution was initially applied to welding, its application to laser deposition was first carried out by Dykhuizen and Dobranich [4]. Vasinonta *et al.* subsequently used the Rosenthal solution to guide the development of process maps relating laser deposition process variables to melt pool size and residual stress [5, 6]. The present authors have adopted a similar approach to the development of thermal process maps for predicting solidification microstructure in laser deposited materials [7–9]. While the authors' prior work has been limited to a point heat source, the current study extends the approach to include the effect of a distributed heat source on both melt pool geometry and the thermal conditions controlling microstructure. Results suggest that intentional variations in beam width could effect significant changes in melt pool size without affecting microstructure.

Geometries Considered

This study considers both the thin-wall (2-D) and bulky (3-D) geometries of Fig. 1, in which the process variables of interest are the absorbed power αQ and velocity V. In each case, it is assumed that the height h and length L are sufficiently large such that the steady-state Rosenthal solution for a moving point heat source applies [3].

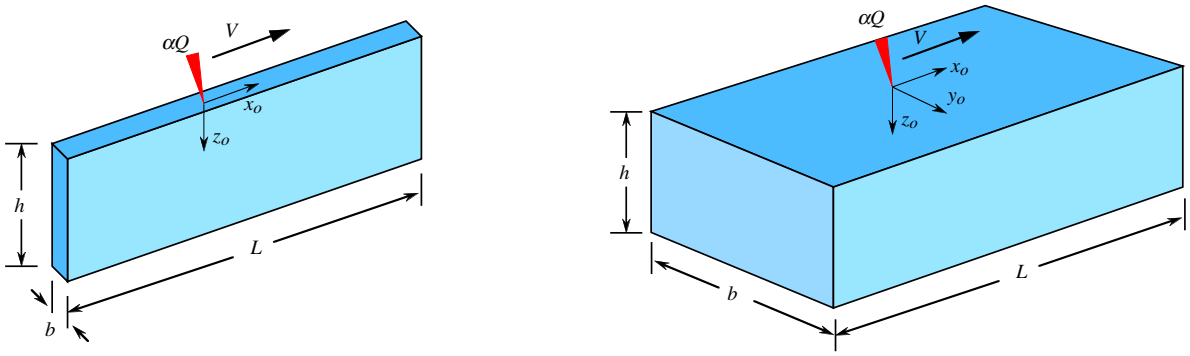

(a) (b)

Figure 1: (a) Thin-Wall and (b) Bulky (3-D) Geometries Considered

Formulation for 2-D Thin Wall Geometry

This section presents the formulation for a uniform power distribution of finite width w by superposition of the 2-D Rosenthal solution for a moving point heat source. The 2-D Rosenthal solution for the quasi-steady-state heat conduction problem of Fig. 1 (a) has been given in dimensionless form by Vasinonta *et al.* [5, 6] as

$$\overline{T} = e^{-\overline{x}_0} K_0 \left(\sqrt{\overline{x}_0^2 + \overline{z}_0^2} \right), \tag{1}$$

where K_0 is the modified Bessel function of the second kind, order zero. The dimensionless variables in eq. (1) are defined in terms of the absorbed laser power αQ and velocity V as

$$\overline{T} = \frac{T - T_0}{\frac{\alpha Q}{\pi k b}}, \quad \overline{x}_0 = \frac{x_0}{\frac{2k}{\rho c V}} \quad \text{and} \quad \overline{z}_o = \frac{z_0}{\frac{2k}{\rho c V}}. \tag{2}$$

In the above normalizations, T is the temperature at a location (x_0,z_0) relative to the moving point heat source and T_0 is the initial temperature of the wall. The relative coordinates (x_0,z_0) are related to fixed spatial coordinates (x, z) at any time t as $(x_0,z_0)=(x-Vt,z)$, where V is the laser velocity. Also in eq. (2), the thermophysical properties ρ, c and k are the density, specific heat and thermal conductivity of the material, which are assumed to be temperature-independent.

When the beam is modeled as a distributed heat source, the absorbed power αQ is distributed over a dimensionless width $\overline{w}$ as shown in Fig. 2 (a). The resulting distributed heat source is $q = \alpha Q/\overline{w}$. In keeping with the spatial normalizations of eq. (2), the normalized beam width is defined as $\overline{w} = w/(2k/\rho cV)$.

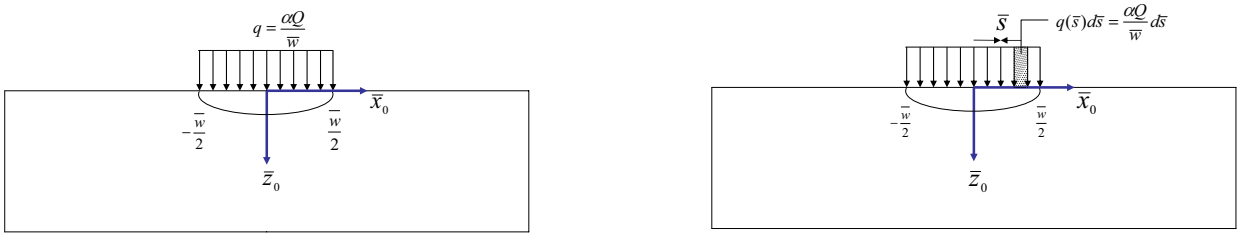

(a) (b)

Figure 2: Uniformly Distributed Heat Source for 2-D Thin Wall Geometry

As illustrated in Fig. 2 (b), the quantity $q(\overline{s})\, d\overline{s}$ acts as a point heat source at a distance $\overline{s}$ from the $\overline{z}_0$ axis. Hence, the solution corresponding to each point heat source $q(\overline{s})\, d\overline{s}$ can be obtained by replacing $\overline{x}_{\rm o}$with $(\overline{x}_{\rm o} - \overline{s})$ in the dimensionless 2-D Rosenthal solution of eq. (1). The total solution is obtained by summing all the point heat sources $q(\overline{s})\, d\overline{s}$ between $-\frac{\overline{w}}{2}$ and $\frac{\overline{w}}{2}$, i.e.,

$$\overline{T} = \frac{1}{\overline{w}} \int_{-\frac{\overline{w}}{2}}^{\frac{\overline{w}}{2}} e^{-(\overline{x}_0 - \overline{s})}\, K_0 \left(\sqrt{(\overline{x}_0 - \overline{s})^2 + \overline{z}_0^2} \right) d\overline{s}\,. \tag{3}$$

Equation (3) represents the dimensionless 2-D Rosenthal solution for an absorbed power αQ uniformly distributed over a beam width w.

Representative Results for 2-D Thin Wall Geometry

This section includes representative dimensionless results which illustrate the effect of beam width on melt pool geometry and microstructure for 2-D thin wall geometries. For the purpose of illustration, attention is restricted to small-scale deposition of Ti-6Al-4V, although more comprehensive results are given in [10]. The values of laser power ($Q = 350$ *W*) and velocity ($V = 4.23$ *mm/s*) considered here fall in the range of powers and velocities that are typical of those used in the $\mathrm{LENS}^{\mathrm{TM}}$ deposition of thin-wall geometries. The thermophysical properties of Ti-6Al-4V are assumed constant at the melting temperature $T_m = 1654°C$, while the absorption coefficient is assumed to be $\alpha = 0.35$. Finally, the wall thickness is assumed constant at $b = 2.26$ *mm*, which is in keeping with that used in the authors' prior published work [7–9,11]. The above values correspond to a dimensionless melting temperature $\overline{T}_m = 2.88$, where

$$\overline{T}_m = \frac{T_m - T_0}{\frac{\alpha Q}{\pi k b}}\,. \tag{4}$$

Effect of Beam Width on Melt Pool Geometry

In order to determine the melt pool geometry (length and depth), the coordinates $(\overline{x}_0, \overline{z}_0)$ which lie on the boundary of the melt pool are determined by replacing $\overline{T}$ with the melting temperature $\overline{T}_m$ and finding the roots of eq. (3) numerically. In so doing, both the numerical integration and root finding are conducted using the software package MATLAB. The resulting normalized melt pool length $\bar{l}$ and normalized melt pool depth $\bar{d}$ are defined as

$$\overline{l} = \frac{l}{\frac{2k}{\rho c V}} \text{ and } \overline{d} = \frac{d}{\frac{2k}{\rho c V}}, \tag{5}$$

which are in keeping with the spatial normalizations of eq. (2).

The normalized melt pool length and depth are plotted as a function of normalized beam width in Fig. 3. For the given velocity and material properties, the results of Fig. 3 correspond to actual beam widths in the range $0 < w < 1.51$ *mm*. The values of normalized melt pool length $\bar{l}$ and normalized melt pool depth $\bar{d}$ along the ordinate $\overline{w} = 0$ correspond to the Rosenthal point source solution, and are in agreement with results previously published in the literature [6, 12, 13].

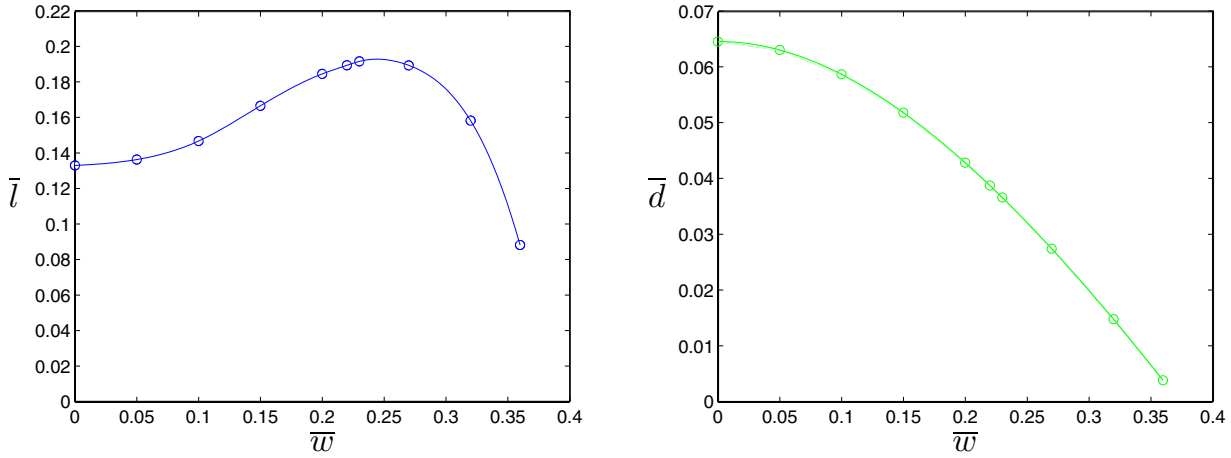

(a) Normalized Melt Pool Length

(b) Normalized Melt Pool Depth

Figure 3: Effect of Normalized Beam Width on (a) Normalized Melt Pool Length and (b) Normalized Melt Pool Depth for $\overline{T}_m = 2.88$

The results of Fig. 3 (a) indicate that the normalized melt pool length initially increases as the laser power is changed from a point source ($\overline{w} = 0$) to a uniformly distributed source of width $\overline{w}$. This is because spreading out the heat source initially heats more material along the length to temperatures above $\overline{T}_m$. This increase in melt pool length continues until it reaches a maximum value at a specific value of $\overline{w}$. At this point, the heat flux becomes insufficient to melt any additional material along the length, so that subsequent increases in $\overline{w}$ result in a decrease in melt pool length. This decrease in melt pool length continues until the heat flux is no longer sufficient to melt any material at all, so that the melt pool ceases to exist ($\overline{l} \to 0$).

In contrast to the normalized melt pool length, the normalized melt pool depth decreases monotonically with increasing $\overline{w}$ (Fig. 3 (b)). While spreading out the heat source initially melts more

material in the length direction, the amount of heat available to melt the material through the depth decreases. As observed for melt pool length, this decrease in melt pool depth continues until the point when the melt pool ceases to exist ($\overline{d} \rightarrow 0$). Inspection of the ordinate scales in Fig. 3 suggests that melt pool depth is more sensitive to changes in beam width compared to melt pool length; however, results also suggest that changing the beam width can have a significant effect on melt pool length, melt pool depth and the overall shape of the melt pool.

Effect of Beam Width on Microstructure

As discussed in [7–9], the microstructure (grain size and morphology) of deposited metals depends on cooling rates and thermal gradients at the onset of solidification (i.e., along the boundary of the melt pool). For the case of a distributed heat source, expressions for the dimensionless cooling rate and thermal gradient can be obtained through analytical differentiation of equation (3), and are given in [10].

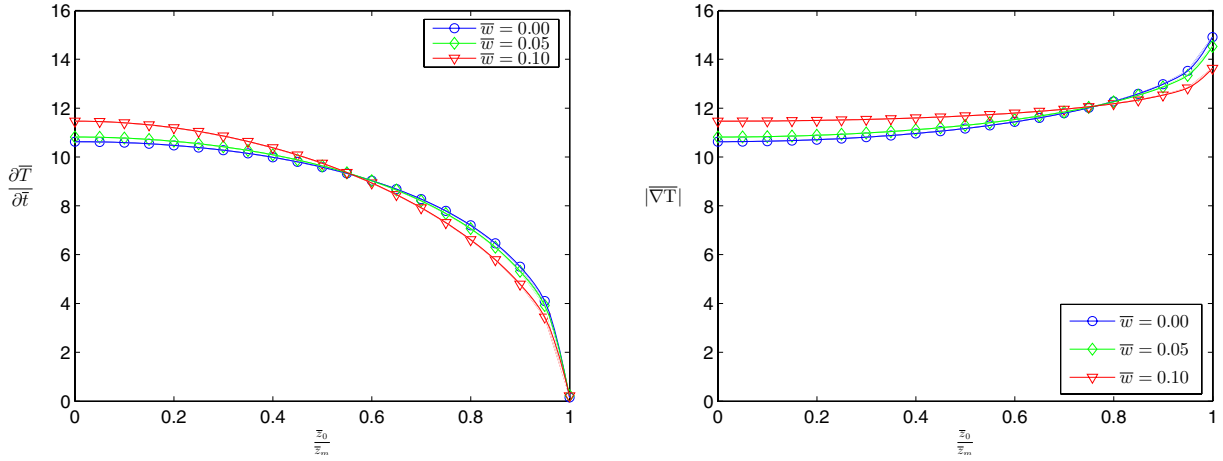

(a) Normalized Cooling Rate

(b) Normalized Thermal Gradient

Figure 4: Effect of Normalized Beam Width on (a) Normalized Cooling Rate (b) Normalized Thermal Gradient for $\overline{T}_m = 2.88$

Representative results for the normalized cooling rate and thermal gradient are plotted in Fig. 4 as a function of relative depth within the melt pool for selected values of the beam width $\overline{w}$. The relative depth within the melt pool varies in the range $0 \leq \overline{z}_0/\overline{z}_m \leq 1$, where $\overline{z}_m$ is the maximum depth of the melt pool for given values of $\overline{T}_m$ and $\overline{w}$. As discussed in [9], the dimensionless cooling rate $\partial\overline{T}/\partial\overline{t}$ is related to the actual cooling rate $\partial T/\partial t$ as

$$\frac{\partial \overline{T}}{\partial \overline{t}} = \left(\frac{2\pi k^2 b}{\alpha Q \rho c V^2} \right) \frac{\partial T}{\partial t}, \tag{6}$$

while the relationship between the dimensionless thermal gradient $\left|\overline{\nabla T}\right|$ and the actual thermal gradient $|\nabla T|$ is given by

$$\left|\overline{\nabla T}\right| = \left(\frac{2\pi k^2 b}{\alpha Q \rho c V} \right) |\nabla T| . \tag{7}$$

In Fig. 4, the curves corresponding to $\overline{w} = 0$ are in agreement with the authors' previous results based on the Rosenthal point source solution [7, 9]. In particular, the results indicate that the solidification cooling rates decrease significantly through the depth of the melt pool, while the thermal gradients (although slightly increasing) are much less sensitive to depth.

The results of Fig. 4 (a) reveal that increasing $\overline{w}$ results in an increase in both thermal gradient and cooling rate up to a certain depth within the melt pool, after which cooling rates and thermal gradients begin to decrease (relative to those for $\overline{w} = 0$). This effect can be explained as follows. For the case of a point source ($\overline{w} = 0$), the left hand boundary of the melt pool (i.e., the solidification boundary) is always relatively far from the heat source. As the laser power is distributed (increasing $\overline{w}$), the solidification front near the surface begins to see the edge of the distributed source, which leads to an increase in both cooling rate and thermal gradient. However, beyond a certain depth within the melt pool (i.e., further away from the edge of the distributed source), bulk heating of the melt pool due to the distributed source results in a decrease in both cooling rate and thermal gradient compared to their point source counterparts. Still, both the solidification cooling rate and thermal gradient appear to be less sensitive to changes in laser beam width compared to the melt pool geometry (length and depth).

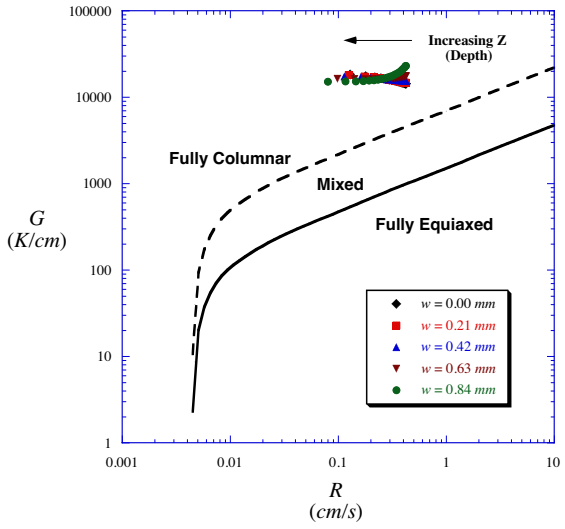

Figure 5: Effect of Beam Width on Predicted Grain Morphology in Ti-6Al-4V
(Thin-Wall Geometry with $Q = 350$ *W*, $V = 4.23$ *mm/s*, $b = 2.26$ *mm* and $\alpha = 0.35$)

Effect of Beam Width on Grain Morphology

As discussed in [7–9], results for solidification thermal gradient and cooling rate can be interpreted in the context of a solidification map to provide predictions of grain morphology in Ti-6Al-4V. Given the solidification cooling rate $\frac{\partial T}{\partial t}$ and thermal gradient $G = |\nabla \mathrm{T}|$, the solidification rate R is determined as

$$R = \frac{1}{G}\frac{\partial T}{\partial t}. \tag{8}$$

The expected grain morphology can be predicted as either equiaxed, columnar or mixed by plotting points in G vs. R space (i.e., on the "solidification map"), which has been previously calibrated for Ti-6Al-4V [14].

A solidification map showing the effect of beam width on predicted grain morphology for small-scale (low power) deposition of thin-wall Ti-6Al-4V deposits is shown in Fig. 5. The values of *G* and *R* plotted in Fig. 5 are extracted from the dimensionless cooling rate and thermal gradient plots of Fig. 4, with thermophysical properties at $1654°C$ and process variables as previously noted.

From Fig. 5, it is clear that the data points corresponding to all beam widths fall in the fully columnar region. This result is in keeping with the solidification map predictions previously reported for a point heat source [7–9, 15], as well as with experimental observations for $\mathrm{LENS}^{\mathrm{TM}}$ deposited Ti-6Al-4V [15, 16]. More importantly, the results of Fig. 5 reveal that in contrast to melt pool geometry, solidification grain morphology is insensitive to changes in beam width.

Formulation for Bulky 3-D Geometry

This section presents the formulation for a uniform distribution of power over a circular beam of finite width *w* by superposition of the 3-D Rosenthal solution for a moving point heat source. The formulation for a square beam can be found in [10].

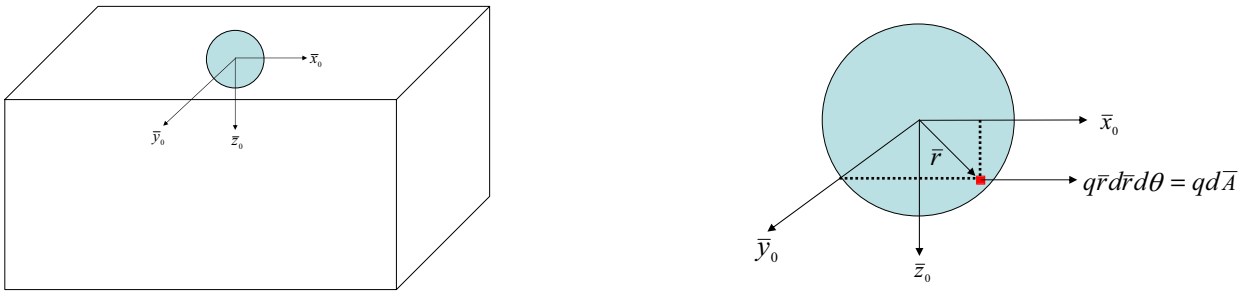

(a) (b)

Figure 6: Uniformly Distributed Heat Source for Bulky 3-D Geometry (Circular Beam Profile)

The 3-D Rosenthal solution for the quasi-steady-state heat conduction problem of Fig. 1 (b) is given in dimensionless form as

$$\overline{T} = \frac{e^{-\left(\overline{x}_0 + \sqrt{\overline{x}_0^2 + \overline{y}_0^2 + \overline{z}_0^2}\right)}}{2\sqrt{\overline{x}_0^2 + \overline{y}_0^2 + \overline{z}_0^2}} \,. \tag{9}$$

The dimensionless variables in eq. (9) are defined in terms of the absorbed laser power αQ and velocity *V* as

$$\overline{T} = \frac{T - T_o}{(\frac{\alpha Q}{\pi k})(\frac{\rho c V}{2k})}, \qquad \overline{x}_o = \frac{x_0}{\frac{2k}{\rho c V}}, \quad \overline{y}_o = \frac{y_0}{\frac{2k}{\rho c V}} \quad \text{and} \quad \overline{z}_0 = \frac{z_0}{\frac{2k}{\rho c V}} \,. \tag{10}$$

The above definition of $\overline{T}$ is in keeping with that used for bulky 3-D geometries in [5, 7, 13, 17], and differs by a factor of 2 from a more recent definition used by other researchers [18–20].

When the beam is modeled as a uniform distributed heat source with a circular beam profile, the absorbed power αQ is distributed over a circle of dimensionless diameter $\overline{w}$ as shown in Fig. 6 (a). The resulting distributed heat source is $q = \alpha Q/(\pi \overline{w}^2/4)$. As illustrated in Fig. 6 (b), the quantity $q\,\overline{r}\,d\overline{r}\,d\theta$ acts as a point heat source at a location $(\overline{r},\,\theta)$ from the origin. Hence, the solution corresponding to each point source $q\,\overline{r}\,d\overline{r}\,d\theta$ can be obtained by substituting $\alpha Q = q\,\overline{r}\,d\overline{r}\,d\theta, \quad \overline{x}_0 = \overline{x}_0 - \overline{r}\cos\theta \quad \text{and} \quad \overline{y}_0 = \overline{y}_0 - \overline{r}\sin\theta$ into the dimensionless 3-D Rosenthal solution of eq. (9). The total solution is obtained by summing all the point heat sources across the circular beam area, i.e.,

$$\overline{T} = \frac{4}{\pi \overline{w}^2} \int_0^{2\pi} \int_0^{\frac{\overline{w}}{2}} \frac{e^{-\left\{(\overline{x}_o - \overline{r}\cos\theta) + \sqrt{(\overline{x}_o - \overline{r}\cos\theta)^2 + (\overline{y}_o - \overline{r}\sin\theta)^2 + (\overline{z}_o)^2}\right\}}}{2\sqrt{(\overline{x}_o - \overline{r}\cos\theta)^2 + (\overline{y}_o - \overline{r}\sin\theta)^2 + (\overline{z}_o)^2}} \overline{r}\,d\overline{r}\,d\theta\,. \tag{11}$$

Equation (11) represents the dimensionless 3-D Rosenthal solution for an absorbed power αQ uniformly distributed over a circular beam of diameter *w*.

Representative Results for Bulky 3-D Geometry

This section includes representative dimensionless results which illustrate the effect of beam diameter on melt pool geometry and microstructure for bulky 3-D geometries. Attention is largely restricted to small-scale deposition of Ti-6Al-4V, while more general results are provided in [10]. The values of laser power ($Q = 550$ *W*) and velocity ($V = 8.47$ *mm/s*) considered here fall in the range of powers and velocities that are typical of those used in LENS$^{\text{TM}}$ deposition of bulky 3-D geometries. Along with Ti-6Al-4V properties at $T_m = 1654°C$, these values of power and velocity correspond to a dimensionless melting temperature $\overline{T}_m = 1.7$, where

$$\overline{T}_m = \frac{T_m - T_0}{\left(\frac{\alpha Q}{\pi k}\right)\left(\frac{\rho c V}{2k}\right)}\,. \tag{12}$$

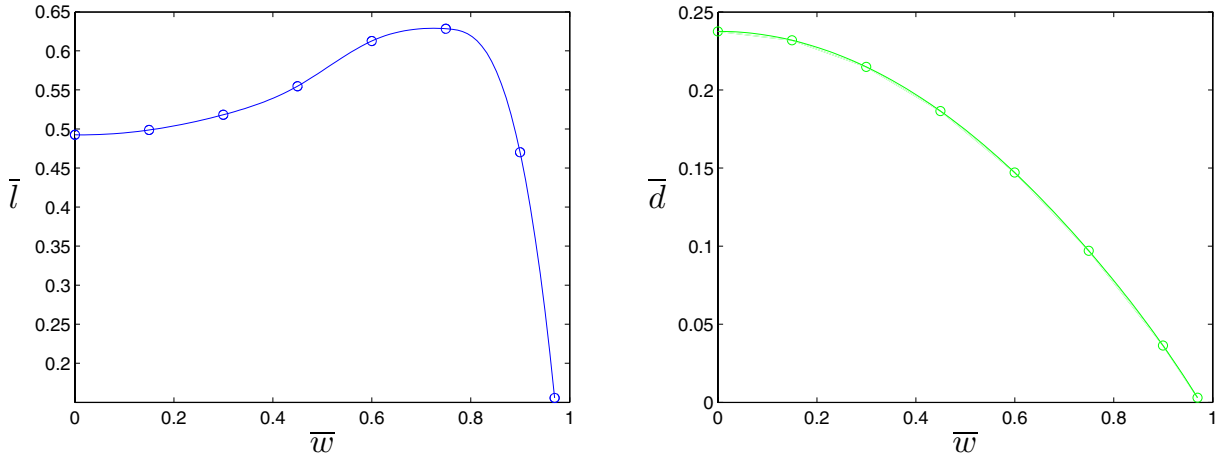

(a) Normalized Melt Pool Length (b) Normalized Melt Pool Depth

Figure 7: Effect of Normalized Beam Width on (a) Normalized Melt Pool Length (b) Normalized Melt Pool Depth for $\overline{T}_m = 1.7$

Effect of Beam Width on Melt Pool Geometry

The normalized melt pool length and depth are plotted as a function of normalized beam diameter in Fig. 7. For the given process variables and material properties, the results of Fig. 7 correspond to actual beam widths in the range $0 < w < 2.0$ *mm*. While trends in the normalized melt pool length and depth are similar to their 2-D counterparts of Fig. 3, the melt pool geometry for bulky 3-D geometries is somewhat less sensitive to variations in beam width. Still, it is clear that variations in beam width can effect significant changes in melt pool geometry for bulky 3-D deposits.

Effect of Beam Width on Microstructure

The expressions for the dimensionless cooling rate and thermal gradient can be obtained through differentiation of eq. (11), and are given in [10]. Representative results for the normalized cooling rate and thermal gradient on the solidification boundary are plotted in Fig. 8 as a function of relative depth within the melt pool for selected values of the beam diameter $\overline{w}$. For bulky 3-D geometries, the dimensionless cooling rate $\partial\overline{T}/\partial\overline{t}$ is related to the actual cooling rate $\partial T/\partial t$ as

$$\frac{\partial\overline{T}}{\partial\overline{t}} = \left(\frac{2k}{\rho cV}\right)^2 \left(\frac{\pi k}{\alpha QV}\right) \frac{\partial T}{\partial t}, \tag{13}$$

while the relationship between the dimensionless thermal gradient $\left|\overline{\nabla T}\right|$ and the actual thermal gradient $|\nabla T|$ is given by

$$\mid \overline{\nabla T} \mid = \left(\frac{2k}{\rho cV}\right)^2 \left(\frac{\pi k}{\alpha Q}\right) \mid \nabla T \mid . \tag{14}$$

Overall, trends in normalized cooling rate and thermal gradient are similar to those previously discussed for 2-D thin wall geometries, with the exception of a slightly anomalous behavior of the cooling rate right at the bottom of the melt pool ($\overline{z}_0/\overline{z}_m = 1$). Whether this is a physical result or simply numerical error is still under investigation.

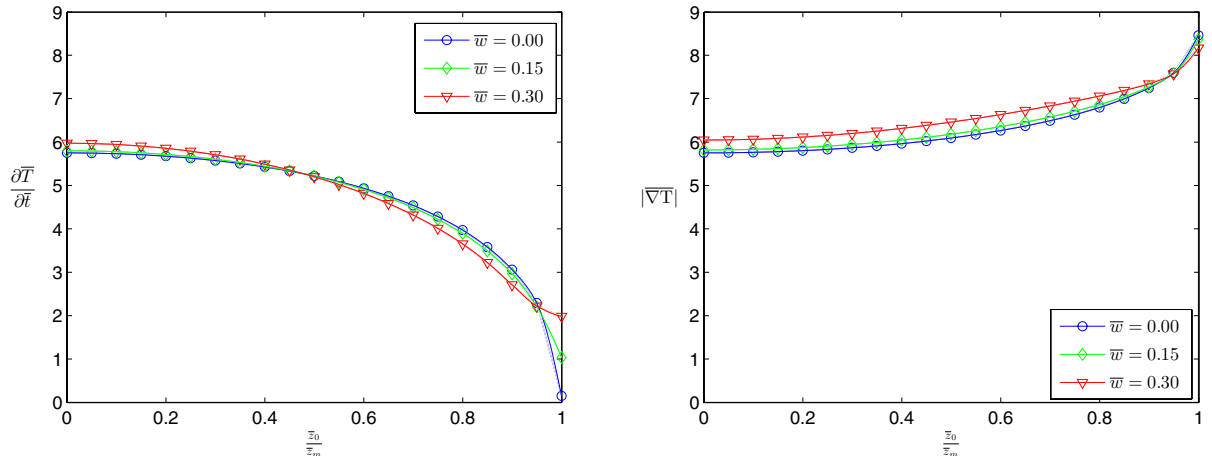

(a) Normalized Cooling Rate (b) Normalized Thermal Gradient

Figure 8: Effect of Normalized Beam Width on (a) Normalized Cooling Rate (b) Normalized Thermal Gradient for $\overline{T}_m = 1.7$

Solidification maps showing the effect of beam width on grain morphology for both small-scale (low power) and large-scale (higher power) deposition of bulky 3-D geometries are shown in Fig. 9. The values of *G* and *R* plotted in Fig. 9 (a) are extracted from the dimensionless cooling rate and thermal gradient plots of Fig. 8, with thermophysical properties of Ti-6Al-4V assumed constant at the melting temperature $T_m = 1654°C$. The values of *G* and *R* plotted in Fig. 9 (b) are extracted from similar cooling rate and thermal gradient plots for a large-scale process (higher power, $\overline{T}_m = 0.06$) that can be found in [10].

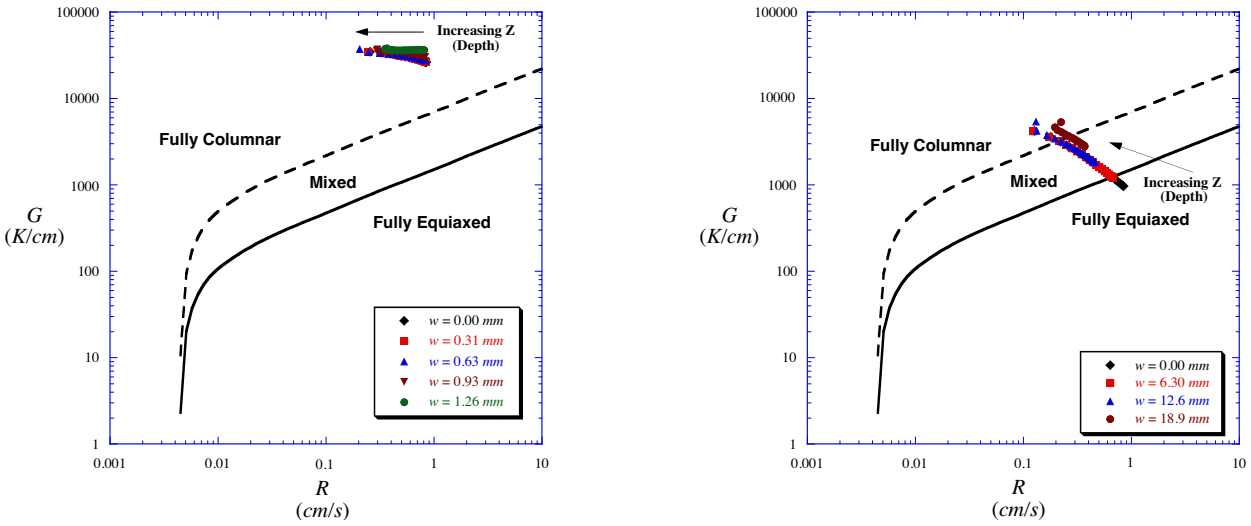

(a) Small-Scale Process

(b) Large-Scale Process

Figure 9: Effect of Beam Width on Grain Morphology in (a) Small- Scale and (b) Large-Scale (Higher Power) Deposition of Bulky 3-D Ti-6Al-4V Deposits

From Fig. 9 (a) (small-scale process), it is clear that the data points corresponding to all beam widths and depths fall in the fully columnar region. This result is in keeping with the solidification map predictions previously reported for a point heat source [7, 8], as well as with experimental observations for LENS^{TM}deposited Ti-6Al-4V [14, 21]. The results of Fig. 9 (b) (large-scale process) suggest the possibility of a graded microstructure through the depth of the deposit, with a mixed or even fully equiaxed microstructure at the surface. This result is again in keeping with the solidification map predictions previously reported for a point heat source [7, 8], as well as with experimental observations reported in the literature for a 14 kW large-scale process [14]. While spreading out the heat source (increasing $\overline{w}$) moves the data slightly toward the fully columnar regime, the results of Fig. 9 appear largely insensitive to variations in beam width.

Summary and Conclusions

The ability to produce parts with required geometric and mechanical properties using beam-based solid freeform fabrication requires an understanding and control of melt pool geometry and microstructure. With the development of electron beam manufacturing or other next-generation beam-based deposition processes, the user may have more precise control over the distribution of incident energy (e.g., beam width). Through superposition of the Rosenthal solution for a moving point heat source, the current study has investigated the effect of beam width on melt pool

geometry (length and depth) and the thermal conditions controlling microstructure (grain size and morphology) for both 2-D thin wall and bulky 3-D geometries. The results of this work suggest that variations in beam width can effect significant changes in melt pool geometry without altering the microstructure.

Acknowledgments

This work has been supported by the National Science Foundation, grant number DMI-0224517, by the joint AFRL/DAGSI Research Program, project number ML-WSU-01-11, and by Wright State University and the Ohio Board of Regents.

References

[1] J. Beuth and N. Klingbeil, "The Role of Process Variables in Laser-Based Direct Metal Solid Freeform Fabrication," *JOM*, pp. 36–39, September 2001.

[2] N. Klingbeil, S. Bontha, D. Gaddam, C. Brown, J. Beuth, A. Birnbaum, and P. Aggarangsi, "Modeling of Melt Pool Size and Solidification Microstructure in Laser-Based Additive Manufacturing," in *Proceedings 2006 NSF DMII Grantees and Research Conference*, (St. Louis, MO), July 2006.

[3] D. Rosenthal, "The Theory of Moving Sources of Heat and Its Applications to Metal Treatments," *Transactions of ASME*, vol. 68, pp. 849–866, 1946.

[4] R. Dykhuizen and D. Dobranich, "Cooling Rates in the LENS Process," *Sandia National Laboratories Internal Report*, 1998.

[5] A. Vasinonta, J. Beuth, and M. Griffith, "Process Maps for Controlling Residual Stress and Melt Pool Size in Laser-Based SFF Processes," in *Solid Freeform Fabrication Proceedings*, (Austin, TX), pp. 200–208, August 2000.

[6] A. Vasinonta, J. Beuth, and M. Griffith, "A Process Map for Consistent Build Conditions in the Solid Freefrom Fabrication of Thin-Walled Structures," *ASME Journal of Manufacturing Science and Engineering*, vol. 123, pp. 615–622, 2001.

[7] S. Bontha and N. Klingbeil, "Thermal Process Maps for Controlling Microstructure in Laser-Based Solid Freeform Fabrication," in *Solid Freeform Fabrication Proceedings*, (Austin, TX), pp. 219–226, August 2003.

[8] N. Klingbeil, S. Bontha, C. Brown, D. Gaddam, P. Kobryn, H. Fraser, and J. Sears, "Effects of Process Variables and Size Scale on Solidification Microstructure in Laser-Based Solid Freeform Fabrication of Ti-6Al-4V," in *Solid Freeform Fabrication Proceedings*, (Austin, TX), August 2004.

[9] S. Bontha, N. Klingbeil, P. Kobryn, and H. Fraser, "Thermal Process Maps for Predicting Solidification Microstructure in Laser Fabrication of Thin Wall Structures," *Journal of Materials Processing Technology*, vol. 178, no. 1-3, pp. 135–142, 2006.

[10] S. Bontha, *The Effect of Process Variables on Microstructure in Laser Deposited Materials*. PhD thesis, Wright State University, 2006.

[11] N.W.Klingbeil, C. Brown, S. Bontha, P. Kobryn, and H. Fraser, "Prediction of Microstructure in Laser Deposition of Titanium Alloys," in *Solid Freeform Fabrication Proceedings*, (Austin, TX), pp. 142–149, August 2002.

[12] A. Vasinonta, J. Beuth, and M. Griffith, "Process Maps for Laser Deposition of Thin-Walled Structures," in *Solid Freeform Fabrication Proceedings*, (Austin, TX), pp. 383–391, August 1999.

[13] A. Vasinonta, *Process Maps for Melt Pool Size and Residual Stress in Laser-Based Solid Freeform Fabrication*. PhD thesis, Carnegie Mellon University, May 2002.

[14] P. Kobryn and S. Semiatin, "Microstructure and Texture Evolution during Solidification Processing of Ti-6Al-4V," *Journal of Materials Processing Technology*, vol. 135, pp. 330–339, 2003.

[15] C. J. Brown, "Modeling of Solidification Microstructure in Laser-Deposited Ti-6Al-4V," Master's thesis, Wright State University, June 2003.

[16] X. Wu, J. Liang, J. Mei, C. Mitchell, P. Goodwin, and W. Voice, "Microstructures of Laser-Deposited Ti-6Al-4V," *Materials and Design*, vol. 25A, pp. 137–144, 2004.

[17] A. Vasinonta, J. Beuth, and R. Ong, "Melt Pool Size Control in Thin-Walled and Bulky Parts via Process Maps," in *Solid Freeform Fabrication Proceedings*, (Austin, TX), pp. 432–440, August 2001.

[18] A. Birnbaum, J. Beuth, and J. Sears, "Scaling Effects in Laser-Based Additive Manufacturing Processes," in *Solid Freeform Fabrication Proceedings*, (Austin, TX), August 2004.

[19] A. Birnbaum, P. Aggarangsi, and J. Beuth, "Process Scaling and Transient Melt Pool Size Control in Laser-Based Additive Manufacturing Processes," in *Solid Freeform Fabrication Proceedings*, (Austin, TX), pp. 328–340, August 2004.

[20] P. Aggarangsi, J. Beuth, and D. Gill, "Transient Changes in Melt Pool Size in Laser Additive Manufacturing Processes," in *Solid Freeform Fabrication Proceedings*, (Austin, TX), August 2004.

[21] P. Kobryn and S. Semiatin, "The Laser Additive Manufacture of Ti-6Al-4V," *JOM*, vol. 53, no. 9, pp. 40–42, 2001.